Supplementary Information (SI)

Large area efficient interface layer free monolithic perovskite/homo-junction-silicon tandem solar cell with over 20% efficiency

Jianghui Zheng[1, †,*], Cho Fai Jonathan Lau[1,†], Hamid Mehrvarz[1,†], Fa-Jun Ma[1], Yajie Jiang[1], Xiaofan Deng[1], Anastasia Soeriyadi[1], Jincheol Kim[1], Meng Zhang[1], Long Hu[1], Xin Cui[1], Da Seul Lee[1], Jueming Bing[1], Yongyoon Cho[1], Chao Chen[2], Martin A. Green[1], Shujuan Huang[1] and Anita W. Y. Ho-Baillie[1,*]

1 Australian Centre for Advanced Photovoltaics, School of Photovoltaic and Renewable Energy Engineering, University of New South Wales (UNSW), Sydney 2052, Australia
2 College of Energy, Xiamen University, Xiamen, 361005, China

[†]These authors contribute equally to this work
* Corresponding Author:
Email: a.ho-baillie@unsw.edu.au (A. Ho-Baillie), jh.zheng@unsw.edu.au (J. Zheng)

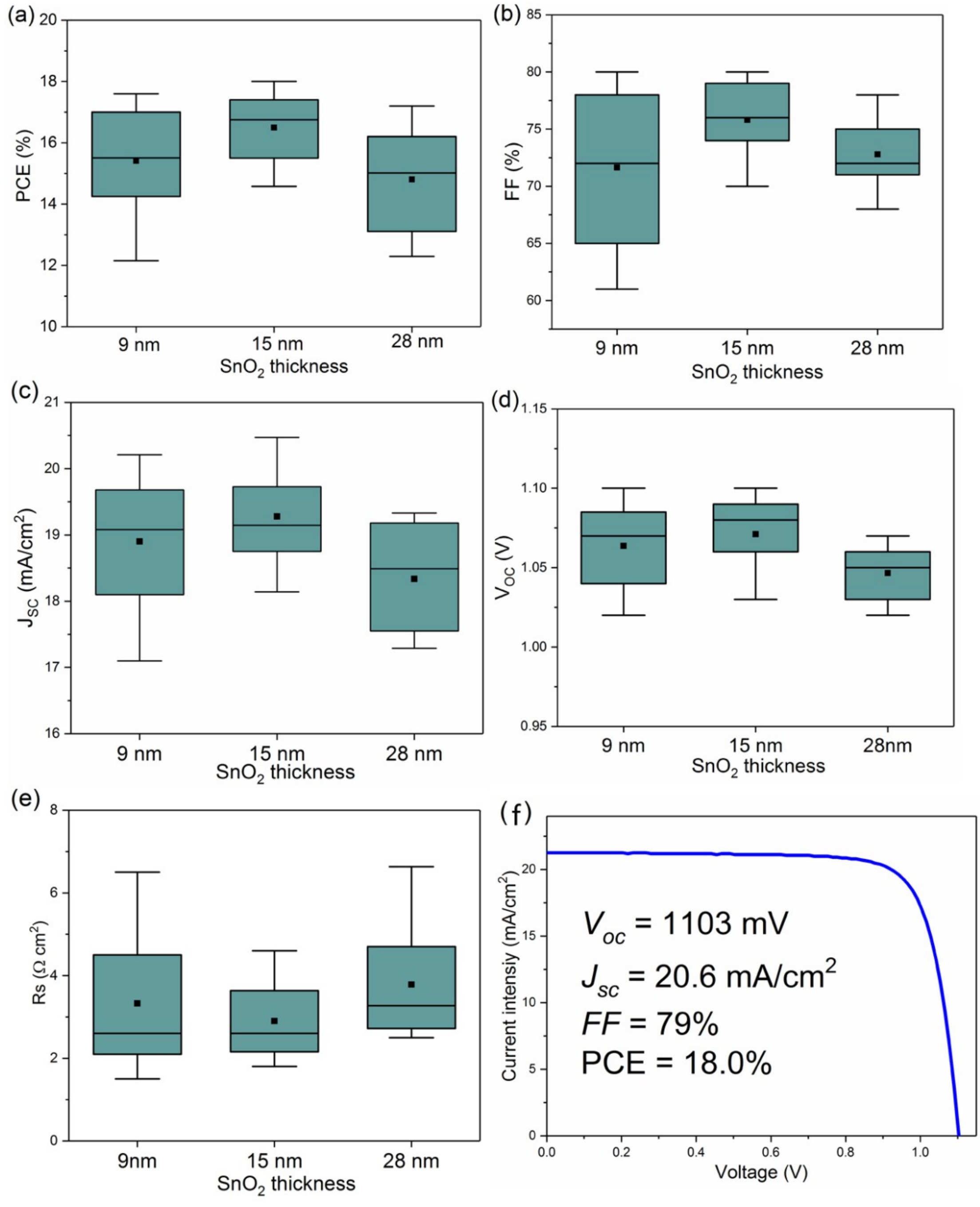

Fig. S1 (a) PCE, (b) FF, (c)J_{SC}, (d)V_{OC}, (e)*Rs* distributions for 12 opaque Au/ /spiro-OMeTAD/$MAPbI_3$/SnO_2/ITO glass PSC with different SnO_2 thickness. The highest value is a maximum value. The highest bar is the 75th percentile value. The middle bar is the median value. The square mark is for average. The lowest bar is the 25th percentile value. The lowest value is the minimum. (f) *J-V* curve of the champion PSC device (with 0.159 cm^2 active area) based on 15 nm SnO_2 ETL.

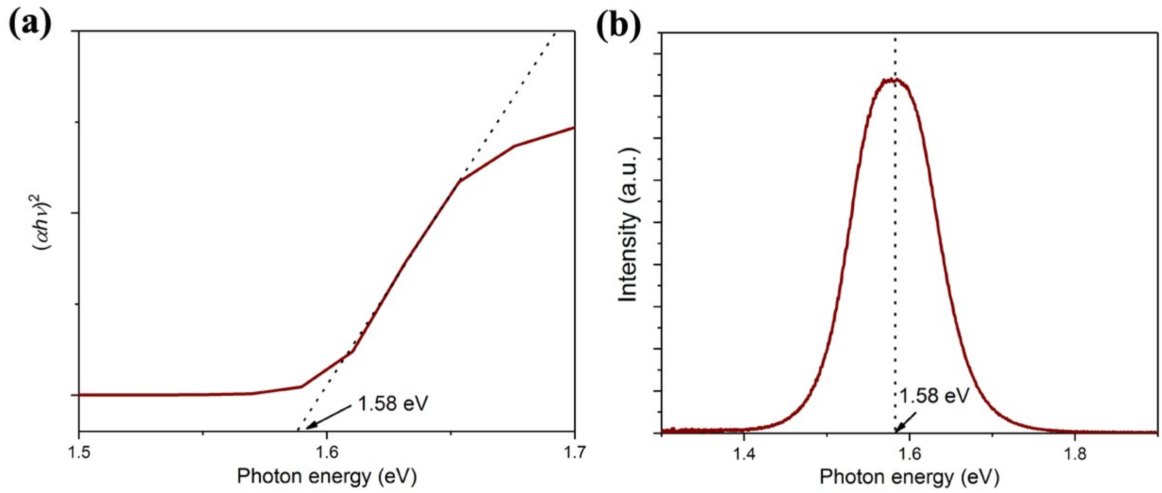

Fig. S2 Tauc plot and PL emission spectrum of $CH_3NH_3PbI_3$ perovskite layer deposited by 2-step method.

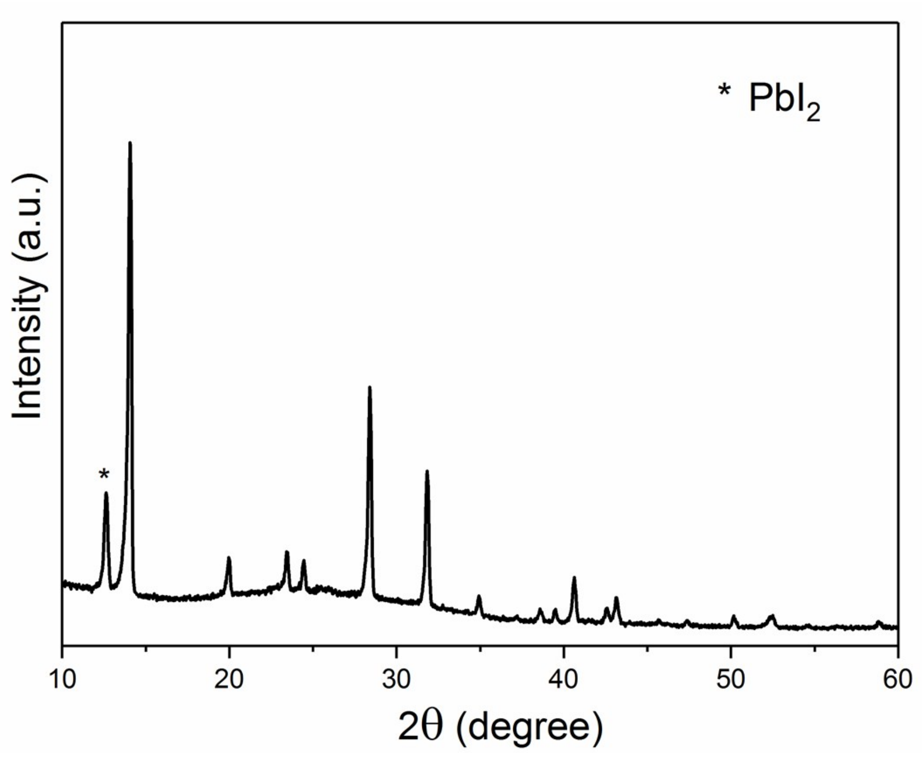

Fig. S3 XRD pattern of $CH_3NH_3PbI_3$ layer deposited by 2 step method on glass.

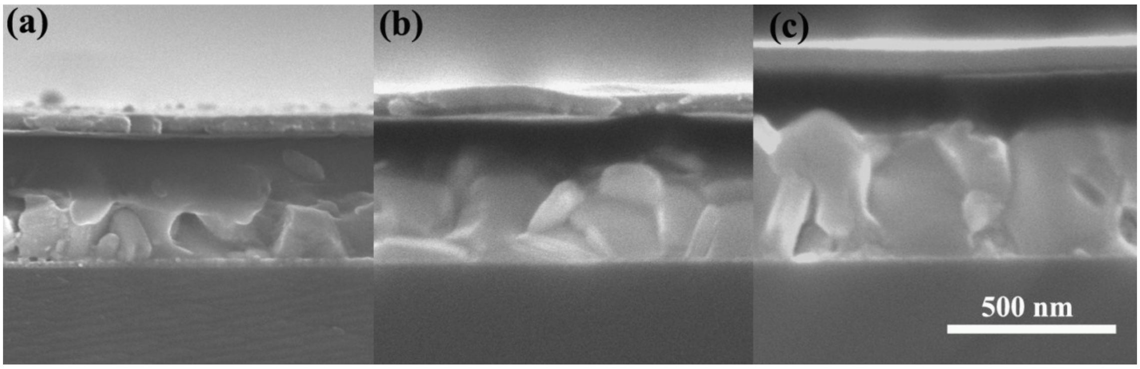

Fig. S4 Cross sectional SEM images of the tandem devices with different thicknesses of $CH_3NH_3PbI_3$ perovskite layer at (a) 260 nm; (b) 380 nm; (c) 470 nm.

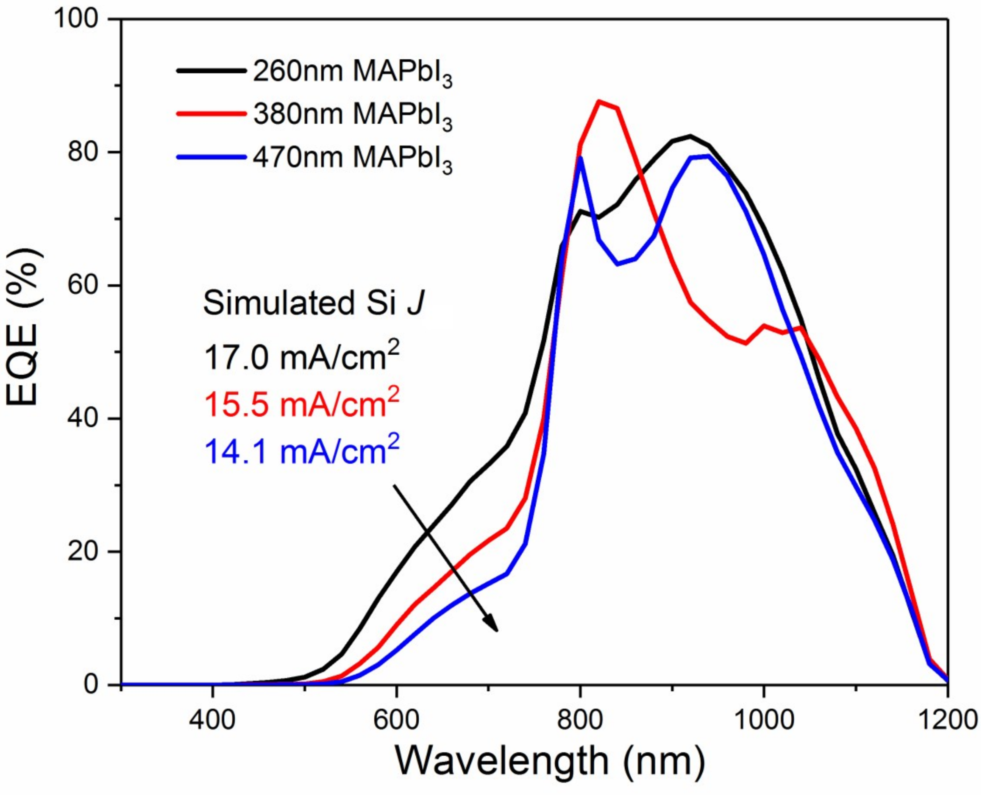

Fig. S5 Simulated the EQE response of bottom silicon cell by changing the $MAPbI_3$ thickness. Note that the SunSolveTM ray tracing package does not allow for carrier recombination input and therefore 100% IQE is assumed for both top perovskite and bottom silicon solar cells which is not the case for experimental cells.

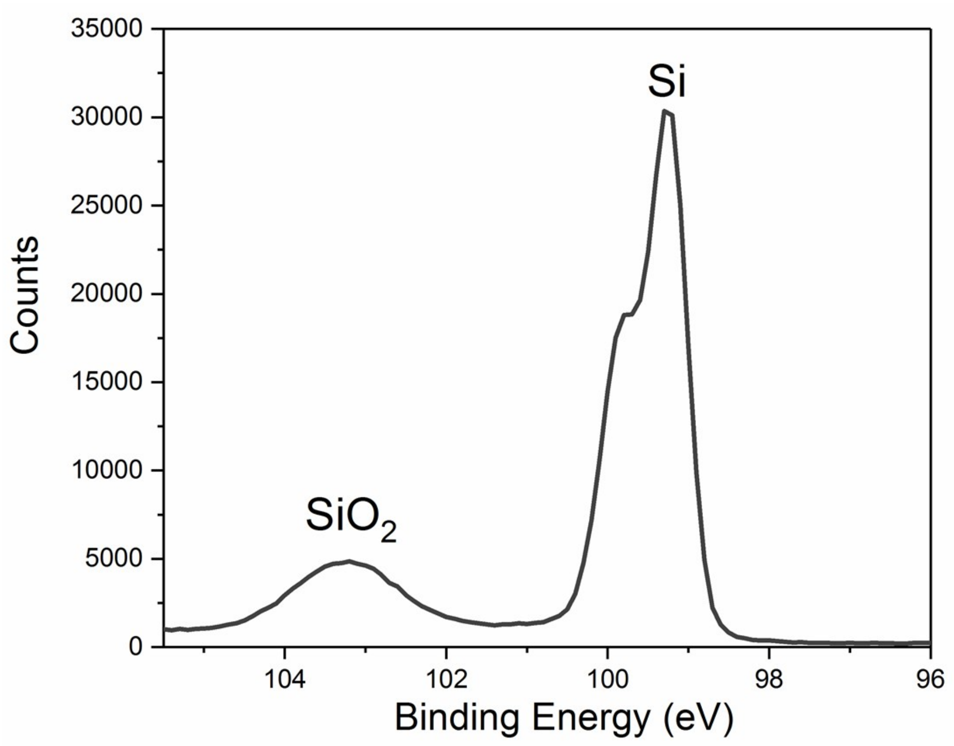

Fig. S6. XPS Si 2p spectrum of silicon surface after UVO treatment. The peak at 103.3 eV is attributed to SiO_2 formed after UVO treatment, while the peak at 99.3 eV is detected from the Si substrate underneath the thin oxide surface [10].

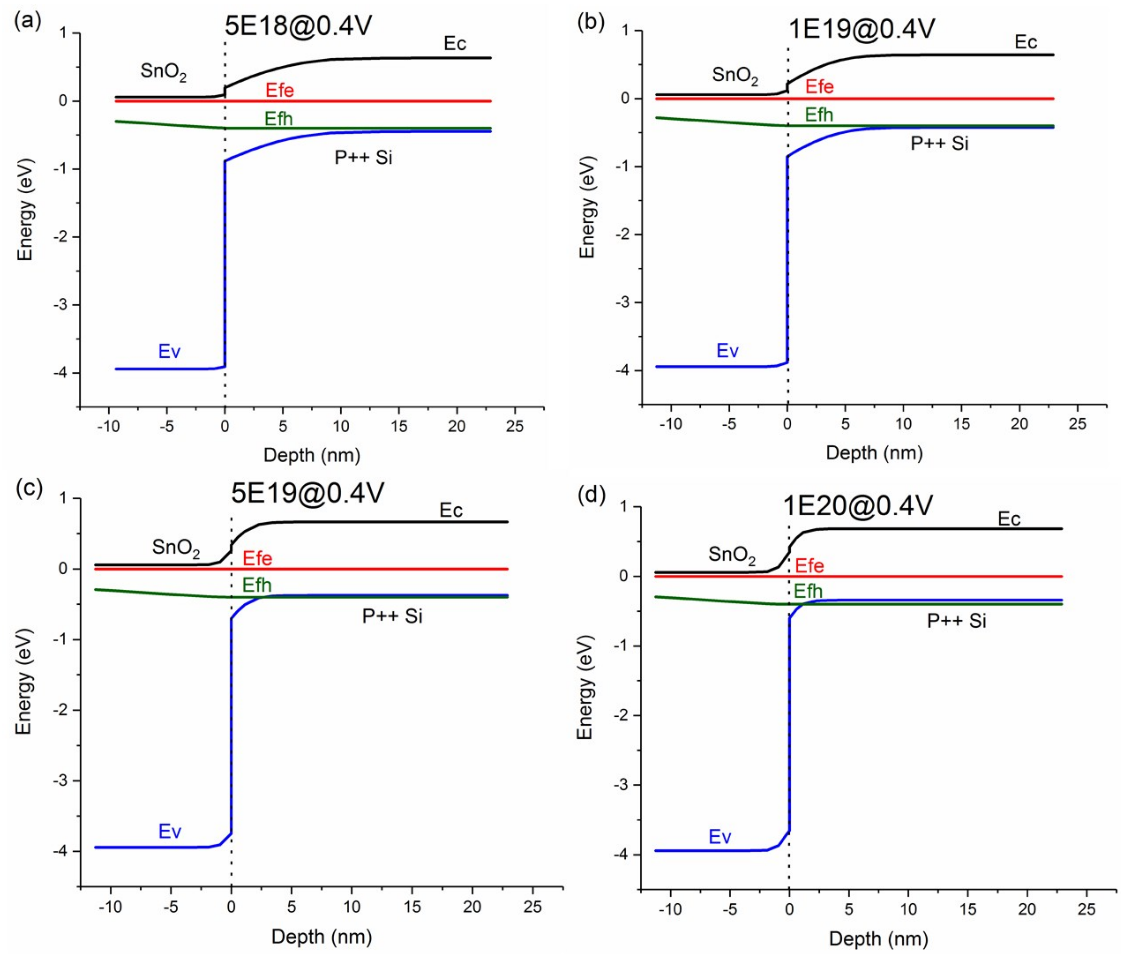

Fig. S7 Band diagrams of SnO_2 and Si interface at the bias voltage of 0.4 V with different p++ doping concentration.

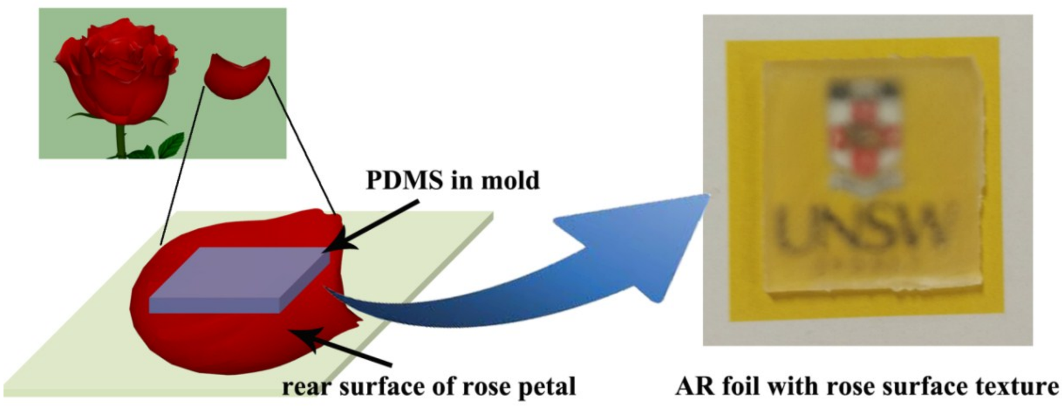

Fig. S8 AR foil fabrication process using rose petal. The thickness of the PDMS AR foil is around 2 mm.

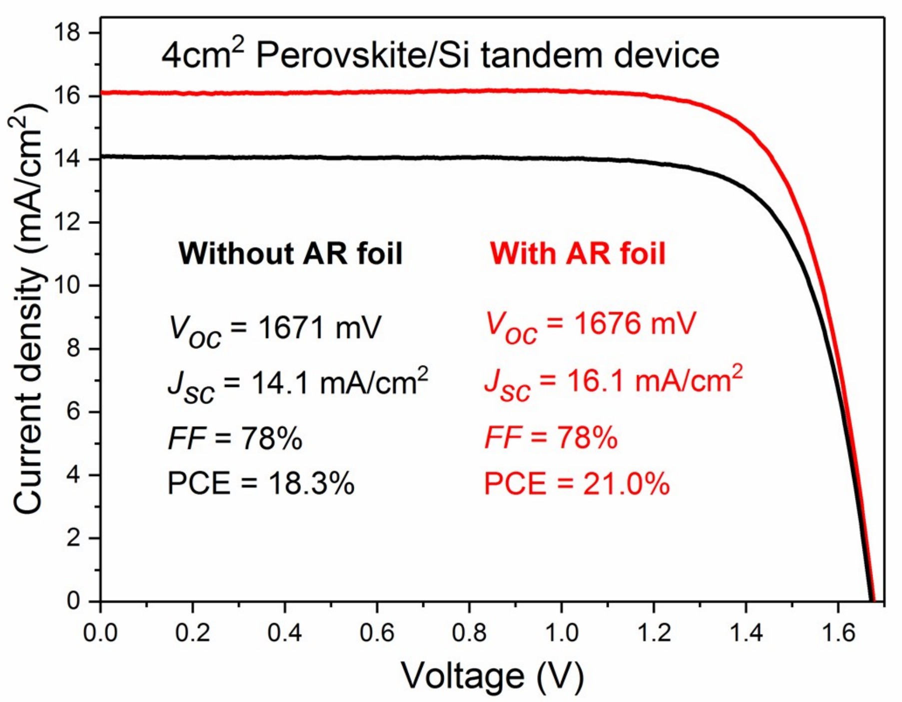

Fig. S9 Reverse scan J-V curve of the 4 cm^2 tandem device using heavier p++ front emitter for the Si bottom cell before (black) and after (red) the use of antireflection foil on the front of the tandem.

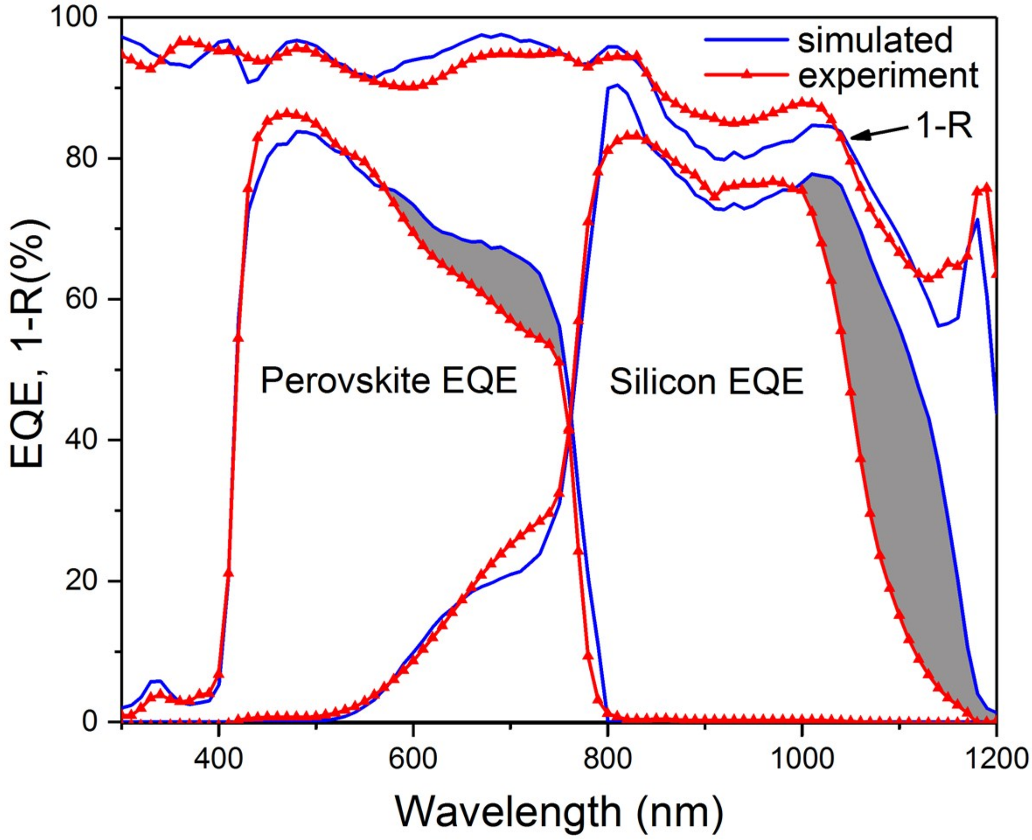

Fig. S10 Simulated (solid line) and experimental (dotted line) EQE and 1-R for the demonstrated perovskite/silicon tandem. Note that the SunSolveTM ray tracing package does not allow for carrier recombination input and therefore 100% IQE is assumed for both top perovskite and bottom silicon solar cells although it is not the case for experimental cells.

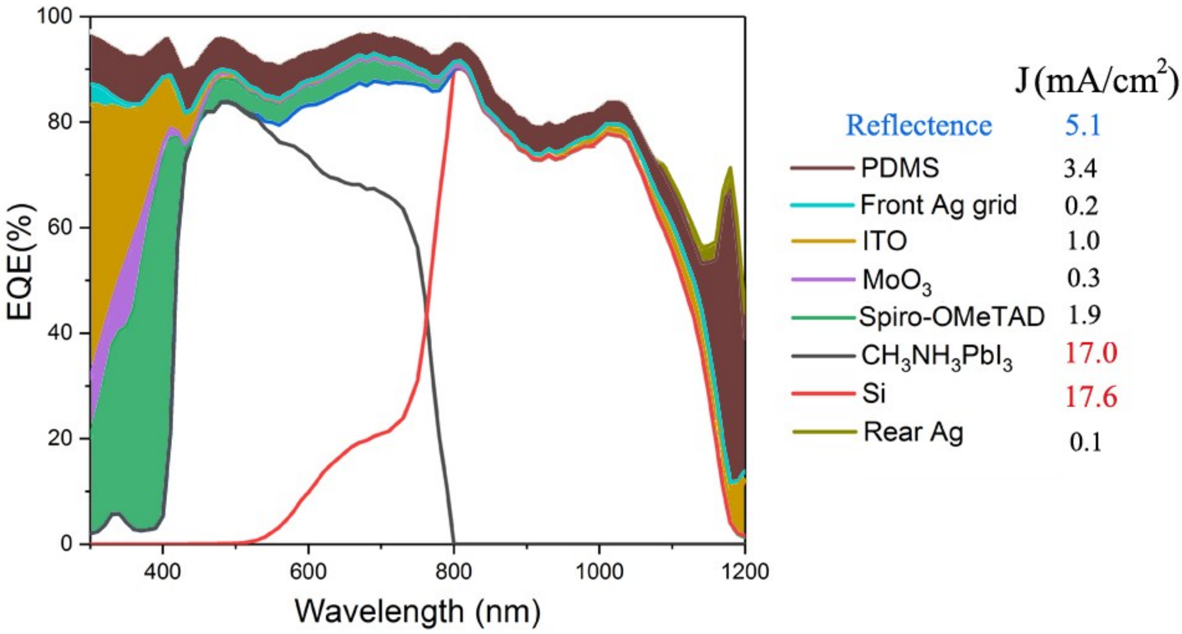

Fig. S11 Optical losses from each layer in the monolithic perovskite/silicon tandem.

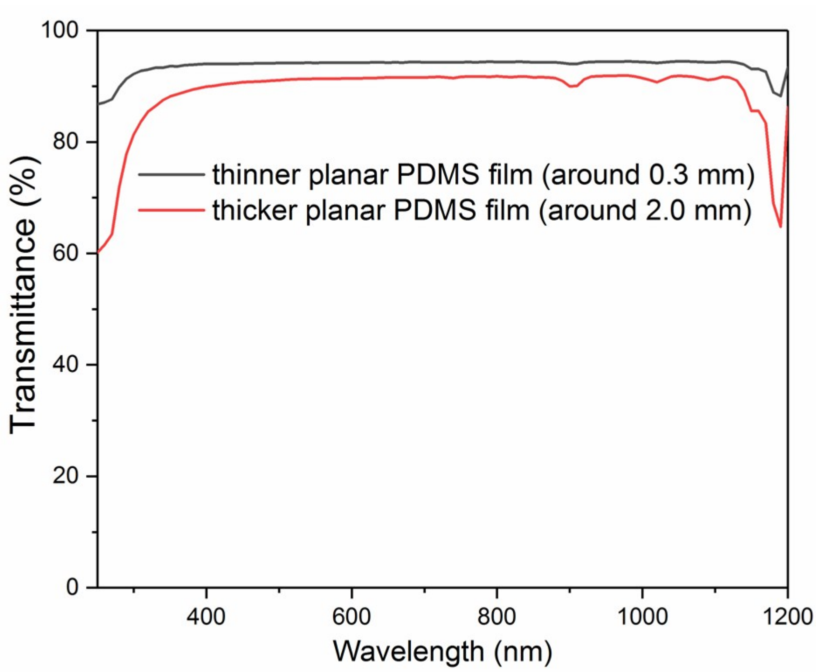

Fig. S12 Measured transmittance of planar thin (0.3 mm) and thick (2.0 mm) PDMS layer showing the optical improvement from the use of thinner PDMS layer.

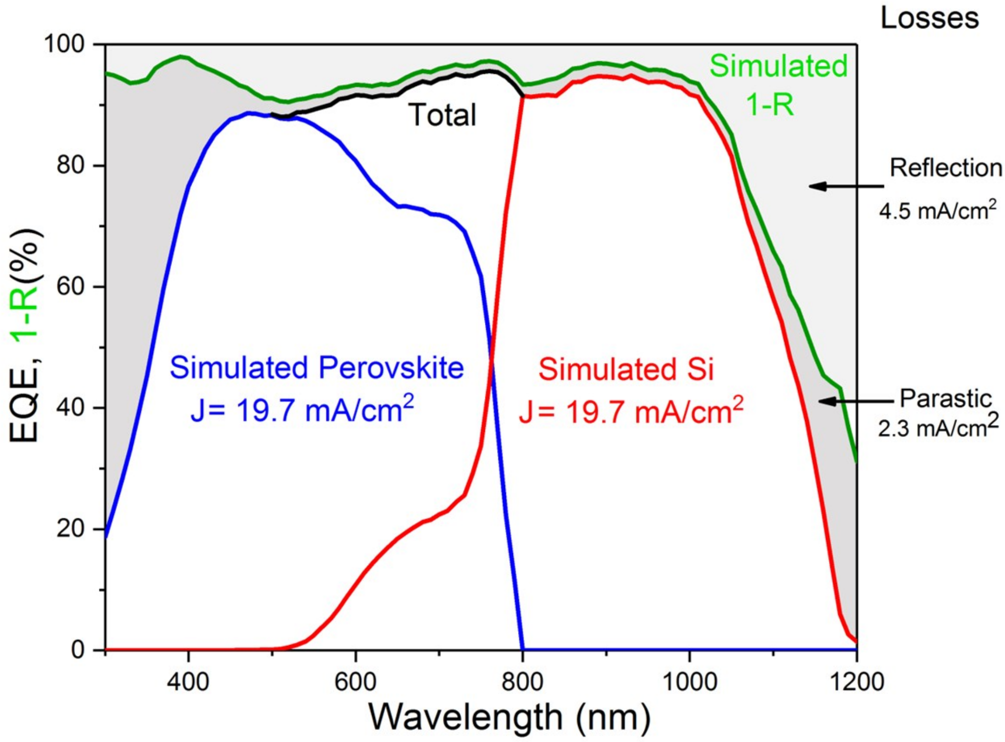

Fig. S13 Simulated EQE and total absorbance (1-reflectance; green line) of improved monolithic cell structure AR foil/Ag grid/ITO/NiO_x/$MAPbI_3$/SnO_2/Silicon/SiO_2/Ag.

Table S2: Breakdown of optical losses for the improved cell structure AR foil/Ag grid/ITO/NiO_x/$MAPbI_3$/SnO_2/Silicon/SiO_2/Ag

Cell	Layers	Thickness	J_A (mA/cm^2)
Perovskite top cell	PDMS foil	0.3 mm	0.6
	Front Ag grid	220 nm	0.2
	ITO	100 nm	1.3
	NiO_x	20 nm	0.2
	$CH_3NH_3PbI_3$	381 nm	***19.7***
	SnO_2	15 nm	0
Silicon bottom	Silicon	300 µm	***19.7***
	SiO_2	160 nm	0
	Rear Ag	2 µm	0.2

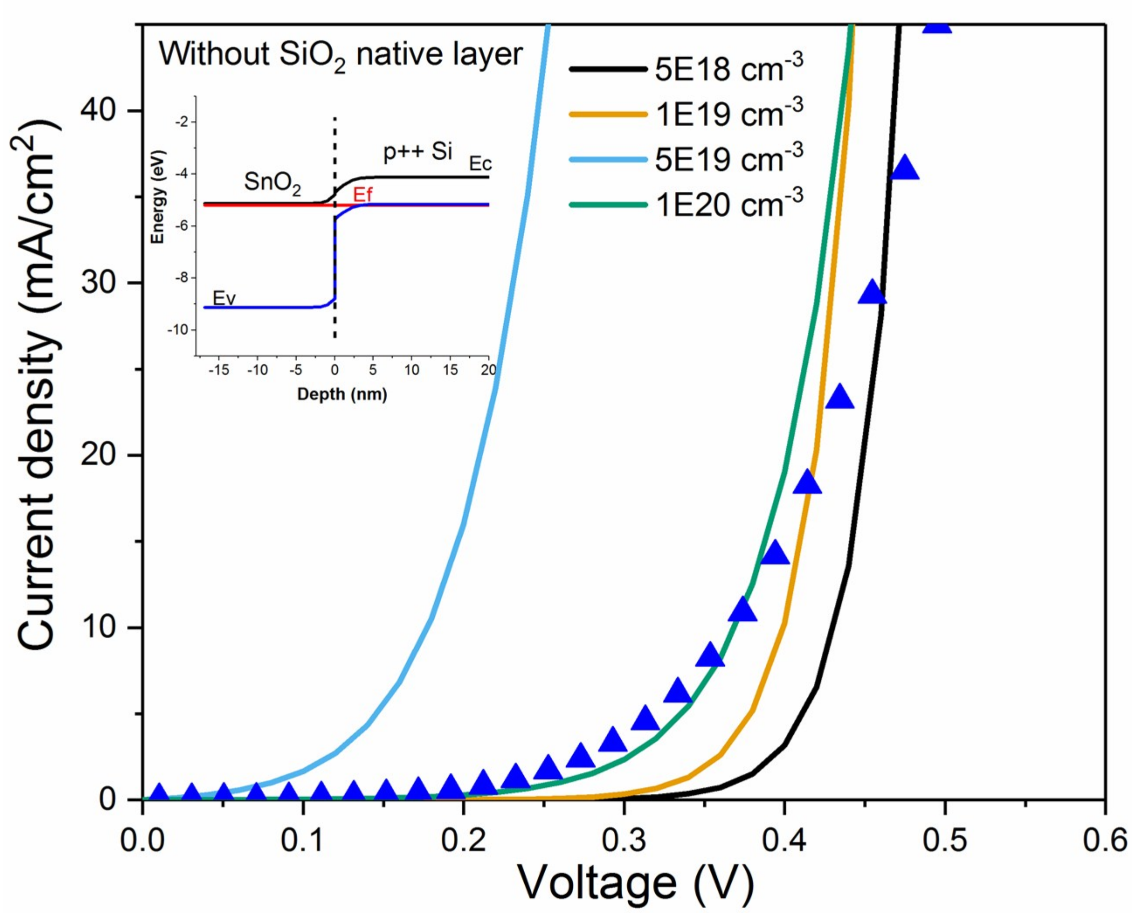

Fig. S14 Simulated dark *I-V* curves for the SnO_2/p++silicon interface without the presence of a native SiO_2 when p++ doping concentration is varied. Inset: corresponding band diagram.

Table S1 Summaries of monolithic 2-terminal perovskite/silicon tandem device.

Perovskite	**Eg (eV)**	**Silicon**	**Interface layer**	**V_{oc} (V)**	**J_{sc} (mA/cm^2)**	***FF***	**PCE (%)**	**Stabilized PCE (%)**	**Area (cm^2)**	**Institute**	**Publish month and Ref**
$MAPbI_3$	1.55	Homojunction	n++ Si tunnel	1.58	11.5	0.75	-	13.7	1.00	MIT/Stanford	2015.03 [1]
$MAPbI_3$	1.55	Homojunction	ZTO	1.64	15.3	0.65	16.3	16.0	1.43	EPFL	2016.12 [2]
$CsRbFAMAPbI_{3-x}Br_x$	1.62	Homojunction	ITO	1.75	17.6	0.74	22.8	22.5	1.00	ANU	2017.10 [3]
$MAPbI_3$	**1.58**	**Homojunction**	**-**	**1.68**	**16.1**	**0.78**	**21.0**	**20.5**	**4.00**	**UNSW**	**This work**
$MAPbI_3$	**1.58**	**Homojunction**	**-**	**1.66**	**15.6**	**0.68**	**17.6**	**17.1**	**<u>16.00</u>**		
$FAMAPbI_{3-x}Br_x$	1.56	HIT	ITO	1.79	14.0	0.77	19.1	18.1	0.16	HZB/EPFL	2015.10 [4]
$MAPbI_3$	1.55	HIT	IZO	1.69	15.9	0.78	20.9	21.2	0.17	EPFL	2015.12 [5]
$MAPbI_3$	1.55	HIT	IZO	1.70	16.1	0.71	19.5	19.2	1.22		
$MAPbI_3$	1.55	HIT	IZO	1.72	16.4	0.73	20.6	20.5	1.43	EPFL	2016.07 [6]
$CsFAPbI_{3-x}Br_x$	1.63	HIT	ITO	1.65	18.1	0.79	23.6	23.6*	1.00	Stanford	2017.02 [7]
$CsFAPbI_{3-x}Br_x$	1.63	HIT	nc-Si tunnel	1.75	16.8	0.76	22.8	22.0	0.25	EPFL	2017.08 [8]
$CsFAPbI_{3-x}Br_x$	1.63	HIT	nc-Si tunnel	1.78	16.5	0.74	21.8	21.2	1.43		
$CsFAPbI_{3-x}Br_x$	1.63	HIT	nc-Si tunnel	1.77	16.5	0.65	19.1	18.0	**<u>12.96</u>**		
$FAMAI_{3-x}Br_x$	1.69	HIT	ITO	1.73	15.3	0.79	20.6	18.0	0.03	PKU	2017.10 [9]

* certified by NREL;

Reference

[1] J.P. Mailoa, C.D. Bailie, E.C. Johlin, E.T. Hoke, A.J. Akey, W.H. Nguyen, M.D. McGehee, T. Buonassisi, A 2-terminal perovskite/silicon multijunction solar cell enabled by a silicon tunnel junction, *Appl. Phys. Lett.,* 2015, **106**, 121105.
[2] J. Werner, A. Walter, E. Rucavado, S.-J. Moon, D. Sacchetto, M. Rienaecker, R. Peibst, R. Brendel, X. Niquille, S. De Wolf, P. Löper, M. Morales-Masis, S. Nicolay, B. Niesen, C. Ballif, Zinc tin oxide as high-temperature stable recombination layer for mesoscopic perovskite/silicon monolithic tandem solar cells, *Appl. Phys. Lett.,* 2016, **109**, 233902.
[3] Y. Wu, D. Yan, J. Peng, T. Duong, Y. Wan, P. Phang, H. Shen, N. Wu, C. Barugkin, X. Fu, S. Surve, D. Walter, T. White, K. Catchpole, K. Weber, Monolithic perovskite/silicon-homojunction tandem solar cell with over 22% efficiency, *Energy Environ. Sci.*, 2017, **10**, 2472-2479.
[4] S. Albrecht, M. Saliba, J.P. Correa Baena, F. Lang, L. Kegelmann, M. Mews, L. Steier, A. Abate, J. Rappich, L. Korte, R. Schlatmann, M.K. Nazeeruddin, A. Hagfeldt, M. Grätzel, B. Rech, Monolithic perovskite/silicon-heterojunction tandem solar cells processed at low temperature, *Energy Environ. Sci.*, 2016, **10**, 81-88.
[5] J. Werner, C.H. Weng, A. Walter, L. Fesquet, J.P. Seif, S. De Wolf, B. Niesen, C. Ballif, Efficient Monolithic Perovskite/Silicon Tandem Solar Cell with Cell Area >1 cm^2, *J. Phys. Chem. Lett.*, 2016, **7**, 161-166.
[6] J. Werner, L. Barraud, A. Walter, M. Bräuninger, F. Sahli, D. Sacchetto, N. Tétreault, B. Paviet-Salomon, S.-J. Moon, C. Allebé, M. Despeisse, S. Nicolay, S. De Wolf, B. Niesen, C. Ballif, Efficient Near-Infrared-Transparent Perovskite Solar Cells Enabling Direct Comparison of 4-Terminal and Monolithic Perovskite/Silicon Tandem Cells, *ACS Energy Lett*., 2016, **1**, 474-480.
[7] K.A. Bush, A.F. Palmstrom, Z.J. Yu, M. Boccard, R. Cheacharoen, J.P. Mailoa, D.P. McMeekin, R.L.Z. Hoye, C.D. Bailie, T. Leijtens, I.M. Peters, M.C. Minichetti, N. Rolston, R. Prasanna, S. Sofia, D. Harwood, W. Ma, F. Moghadam, H.J. Snaith, T. Buonassisi, Z.C. Holman, S.F. Bent, M.D. McGehee, 23.6%-efficient monolithic perovskite/silicon tandem solar cells with improved stability, *Nat. Energy*, 2017, **2**, 17009.
[8] F. Sahli, B.A. Kamino, J. Werner, M. Bräuninger, B. Paviet-Salomon, L. Barraud, R. Monnard, J.P. Seif, A. Tomasi, Q. Jeangros, A. Hessler-Wyser, S. De Wolf, M. Despeisse, S. Nicolay, B. Niesen, C. Ballif, Improved Optics in Monolithic Perovskite/Silicon Tandem Solar Cells with a Nanocrystalline Silicon Recombination Junction, *Adv. Energy Mater.*, 2017, **8**, 1701609.
[9] R. Fan, N. Zhou, L. Zhang, R. Yang, Y. Meng, L. Li, T. Guo, Y. Chen, Z. Xu, G. Zheng, Y. Huang, L. Li, L. Qin, X. Qiu, Q. Chen, H. Zhou, Toward Full Solution Processed Perovskite/Si Monolithic Tandem Solar Device With PCE Exceeding 20%, *Solar RRL*, 2017, **1**, 1700149.

[10] J. F. Moulder, W. F. Stickle, P. E. Sobol, and K. D. Bomben, Handbook of X-ray Photoelectron Spectroscopy, Perkin-Elmer Corp, USA (1992).